Published in final edited form as:
J Neuroimmunol. 2009 June 25; 211(1-2): 73–83. doi:10.1016/j.jneuroim.2009.03.016.

Influenza Virus- and Cytokine-Immunoreactive Cells in the Murine Olfactory and Central Autonomic Nervous Systems before and after Illness Onset

Victor H. Leyva-Grado, **Lynn Churchill**, **Melissa Wu**, **Timothy J. Williams**, **Ping Taishi**, **Jeannine A. Majde**, and **James M. Krueger***
Department of Veterinary and Comparative Anatomy, Pharmacology and Physiology, Washington State University, Pullman, WA 99164

Abstract

Influenza virus invades the olfactory bulb (OB) and enhances cytokine mRNAs therein at the time of illness onset. Here we show that viral antigen immunoreactivity co-localized with glial markers in the OB but could not be detected in other brain areas. Interleukin 1β- and tumor necrosis factor α-immunoreactivity co-localized with neuronal markers in olfactory and central autonomic systems, and the number of cytokine-immunoreactive neurons increased at the time of illness onset [15 h post-inoculation (PI)] but not before (10 h PI). These results suggest that the OB virus influences the brain cytokines and therefore the onset of illness.

Keywords

Influenza virus; Olfactory system; Glia; Neuronal cytokines; Acute phase response; NeuN

1. Introduction

Clinical influenza infections are commonly marked by severe systemic illness both in animals and humans. It is generally assumed that this illness results from cytokines secreted from infected respiratory tissues (Vacheron et al., 1990; Hennet et al., 1992) acting upon the brain. However, we recently demonstrated that a mouse-adapted human strain of influenza (A/Puerto Rico/8/34 or PR8) invades the olfactory bulb (OB) of the brain within 4 h following intranasal infection of mature mice. This finding was unexpected because others have looked for PR8 virus in the mature mouse brain early in the infection with no success (Schlesinger, 1950; Schlesinger et al., 1998; Iwasaki et al., 2004) though it is detected together with viremia at 5 days post-infection (PI) (Mori et al., 1995). Unlike avian influenza strains, PR8, as well as other human influenza strains [with the exception of neuro-adapted human strains (Schlesinger et al. 1998)], are generally considered to be unable to invade the brain of the mature mouse. In our PR8 mouse model we see a precipitous and profound fall in body temperature (hypothermia) at 13–15 h PI along with expression of viral antigens in the rostral OB (Majde

*CORRESPONDING AUTHOR: James M. Krueger, Department of VCAPP, College of Veterinary Medicine, Washington State University, PO Box 646520; Pullman, WA 99164-6520, EMAIL: E-mail: krueger@vetmed.wsu.edu, PHONE: 509-335-8212, FAX: 509-335-6450.

et al., 2007). This hypothermic response, which is characteristic of mouse influenza (Fang et al., 1995; Conn et al., 1995), marks the onset of illness [often termed sickness behavior or the acute phase response (APR)] in lethal PR8 influenza models.

Viral RNA and proinflammatory cytokine interleukin-1β (IL1β) and tumor necrosis factor-α (TNFα) transcripts are also up-regulated in the OB at the time of illness onset, along with mRNAs of type I interferon-induced enzymes (Majde et al., 2007). The viral RNA consists of virion RNA (minus strand) and replication intermediates (plus strand), indicating that at least partial viral replication is ongoing in the OB as early as 4 h (Majde et al., 2007). By 15 h PI, viral antigens are detected in microglia-like cells within the olfactory nerve (ON) and in the glomerular layer (GL) (Majde et al., 2007). However, characterization of the cell types containing viral antigen and cytokine proteins remains incomplete.

Brain regions with projections from the OB, particularly the hypothalamus, are known to be involved in APRs such as hypothermia. The amygdala influences the APR via the hypothalamic-pituitary-adrenal axis (Xu et al., 1999; Lin and York, 2004). Specifically, activation of the central amygdala (CeA), as evidenced by an increase of c-Fos or cytokines such as TNFα and IL1β, occurs after immunological challenges in rodents by herpes virus (Ben Hur et al., 1996), systemic Gram-negative toxins such as lipopolysaccharide (LPS) (Frenois et al., 2007), Gram-positive enterotoxins (Rossi-George et al., 2005), or the cytokine IL-1β (Xu et al., 1999). After systemic or local injections with LPS or IL-1β, there is also an increase in c-Fos-IR in the hypothalamic arcuate nucleus (Arc) (Reyes and Sawchenko, 2002; Scarlett et al; 2007). Microinjection of IL1 into the medial preoptic nucleus (MPO) increased body temperature in rats (Sellami and de Beaurepaire, 1995). The Arc may also have a role in initiating the APR (Reyes and Sawchenko, 2002). Although such data indicate that the amygdala and hypothalamus play a role in the APR, it remains unknown whether the olfactory pathway is important in early APR ontogenesis.

In this report we investigate by immunohistochemistry (IHC) the distribution of viral antigen and the proinflammatory cytokines IL1β and TNFα in cells of the OB, the olfactory cortex [including the piriform cortex (Pir) and olfactory tubercle (Tu)], the somatosensory cortex (Sctx) and components of the central autonomic nervous system region, i.e., the amygdala [specifically the basolateral amygdala (BLA) and the CEA] and the hypothalamus (specifically the Arc and MPO). Infected or control mice were euthanized prior to illness onset (10 h PI), or after the onset of the hypothermic response to influenza virus at 15 h PI (Majde et al., 2007), and cells expressing viral and cytokine antigens were examined. Cells expressing cytokines were counted by light microscopy and cells expressing viral antigen or cytokines were examined for glial or neuronal markers by light or confocal microscopy. Viral antigen was localized in glial cells in the ON and GL of the OB. At the time of illness onset, but not earlier, we detected an increased number of proinflammatory cytokine-expressing olfactory and central autonomic neurons. Collectively, these observations suggest that viral invasion of the OB could ultimately be responsible for, or contribute to, the onset of viral illness through cytokine-modulated neuronal pathways projecting to the hypothalamus.

2. Materials and Methods

2.1. Mice

C57BL/6 male mice 4–6 weeks of age were purchased from Jackson Laboratories (Bar Harbor, ME). They were used in the experiments when they were 8–12 weeks of age. After arrival, animals were quarantined and subsequently housed in 48 × 25 × 16 cm polypropylene cages with filter tops to minimize intercurrent infections. Food and water were provided *ad libitum*. Mice were maintained on a 12:12 h light: dark cycle at an ambient temperature of 24° ± 1°C. Institutional guidelines for the care and use of research animals were followed and

protocols were approved by the Washington State University Institutional Animal Care and Use Committee.

Two groups of mice (total 24) were used in this experiment. One group was sacrificed at 10 h PI after receiving boiled (n=6) or live (n=6) virus and another group was sacrificed at 15 h PI after receiving boiled (n=6) or live (n=6) virus.

2.2. Virus

Influenza (A/Puerto Rico/8/34, H1N1) virus was supplied by Specific Pathogen-Free Avian Supply (SPAFAS, North Franklin, CT) where the virus was propagated in specific pathogen-free (SPF) chicken embryos and allantoic fluid was harvested using pyrogen-free materials. The virus was purified by sucrose-gradient sedimentation using pyrogen-free materials and the stock was tested for endotoxin and mycoplasma (negative), and titered in Madin Darby canine kidney cells as previously described (Chen et al., 2004).

2.3. Intranasal (IN) inoculation procedure

Mice were inoculated IN at light onset by delivering 25 μl to each nostril using a 100 μl micropipette under light methoxyflurane (Metofane, Schering-Plough Animal Health, Union, NJ) inhalation anesthesia. Infected mice (n=12) received 2.5×10^6 $TCID_{50}$ purified PR8 diluted in Dulbecco's phosphate buffered saline (DPBS). Control mice (n=12) received the same diluted virus that was heat-inactivated prior to the inoculation by suspending the sample in boiling water for 25 min (boiled virus).

2.4. Tissue collection

Mice were returned to their home cages after virus inoculation. Mice were killed at 10 h (prior to hypothermia onset) or at 15 h PI (after hypothermia onset) under deep Metofane anesthesia. The animals were perfused intracardially with warm saline (0.9% NaCl) containing 0.004% of heparin (Celsus laboratories, Cincinnati OH) followed by 35 ml of cold 4% paraformaldehyde in phosphate-buffered saline (PBS). Perfusion was performed using a Masterflex pump model 7014-20 (Cole-Palmer, USA), using a 21 G needle at a flow rate of 2.0 ml/min. Brains were carefully removed from the cribriform plate to maintain an intact OB. Brains were placed in ice-cold 4% phosphate-buffered formaldehyde to post-fix for 6 h, and then were sunk in 20% sucrose overnight. The OBs were separated from the rest of the brain, frozen in crushed dry ice, and stored at −80° C until sectioned.

2.5. Immunohistochemistry (IHC)

OBs, forebrain and midbrain sections were processed in pairs using sections from a mouse inoculated with live virus and sections from another mouse inoculated with boiled virus. Tissue sections were processed as previously reported (Churchill et al., 2005; Majde et al., 2007).

2.5.1. Single labeling for light microscopy (DAB staining)—Adjacent tissue sections were incubated with one of the following antibodies; mouse monoclonal anti-influenza H1N1 virus antibody (Millipore, Bioscience Research Reagents, Temecula, CA, catalog # MAB8261, dilution 1:100), mouse monoclonal anti-influenza nucleoprotein (NP) antibody (Millipore, catalog # MAB8257, dilution 1:100), rabbit anti-recombinant mouse IL1β (Millipore, catalog # AB1413, dilution 1:100), goat anti-recombinant rat TNFα (17 kD secreted form, R&D, Minneapolis MN, catalog # AF-510, dilution 1:200), and rat anti-mouse F4/80 [a macrophage marker that also stains microglia in the OB, Serotec, Raleigh, NC, catalog # MCA497GA, dilution 1:100]. The secondary antibodies were biotinylated horse anti-mouse, anti-rat or anti-goat IgG or biotinylated goat anti-rabbit IgG (Vector Laboratories, Burlingame, CA, dilution

1:500). Sections were stained using diaminobenzidine as a chromophore (DAB kit, Vector, catalog # SK4100).

2.5.2. Double labeling for light and confocal microscopy (fluorescent staining)

—After immersion in 3% blocking serum [a combination of normal chicken serum (NCS) and normal donkey serum (NDS)] for 1 h, adjacent sections were incubated with a mixture of the anti-influenza H1N1 (Millipore, 1:100) and F4/80 (Serotec, 1:100) or rabbit anti-mouse GFAP (an astrocyte marker; Millipore, catalog # MAB360, dilution 1:1000) antibodies prepared in 2% serum (NDS and NCS) at 4°C for 3 days. For double-labeling with the anti-mouse NeuN nuclear protein-neuronal marker (Millipore, dilution 1:1000) we used a polyclonal goat anti-H1N1 antibody (Fitzgerald Industries International, Inc., Concord, MA, catalog # 20IG23, dilution 1:100). Also, adjacent sections were incubated in rabbit anti-mouse IL1β (Millipore, dilution 1:100) in combination with mouse anti-rat F4/80, mouse anti-NeuN, or rabbit anti-mouse GFAP antibodies. Finally, some OB sections were incubated with goat anti-rat TNFα (R&D systems, dilution 1:200) and anti-mouse NeuN antibodies. After incubation, the samples were washed with PBS and then were incubated in the dark for 2 h at room temperature with secondary antibodies using a combination of Alexa Fluor 488 chicken anti-rat (Invitrogen, Carlsbad CA, dilution 1:500), anti-rabbit, or anti-goat, plus Alexa Fluor 555 donkey anti-mouse for the sections with virus antibodies, and a combination of Alexa Fluor 488 chicken anti-rat, anti-rabbit or anti-mouse, plus Alexa Fluor 568 goat anti-rabbit (for the sections with the IL1β antibodies) or donkey anti-goat (for the sections with TNFα antibodies). After incubation the sections were washed and then mounted on gelatin-coated slides, dried, and cover slipped with fluorescent hard set mounting medium (VectaShield-Hard set, Vector, catalog # H-1400).

2.6. Antibody specificity analysis

The antibodies used in this report were used in previous experiments and tested for specificity [McQuillin et al., 1985; Walls et al., 1986 (anti-influenza antigens, according to manufacturer); Stichel and Luebbert, 2007 (F4/80 and TNFα); Barbe et al., 2003 (IL1β)]. We used antiviral monoclonal antibodies made in mouse and secondary biotinylated horse anti-mouse antibodies; consequently, we were not able to determine if the observed immunoreactivity was due in part to the binding of the secondary antibodies to endogenous immunoglobulins attached to activated microglia through Fc receptors (Stangel and Compston, 2001). However, when the primary mouse antibody was omitted, staining by the horse secondary antibody could be distinguished from staining seen when both the primary antibody and secondary antibodies were used. Further, our observations using the goat polyclonal antibody to H1N1 employed for confocal studies showed specific labeling in the OB GL and the ON, and stained microglial cells in the tissues double-labeled with Neu N (see Fig. 6C).

We confirmed IL1β and TNFα antibody specificity by several methods. (1) Weomitted the primary antibody during the immunohistochemistry procedure. (2) Next, pre-absorption experiments were done by overnight incubation of the primary antibody with its target cytokine recombinant rat TNFα (R&D systems) or recombinant mouse IL1β (R&D systems) at a molar ratio of 1:45. The primary antibodies were incubated with the appropriate recombinant protein for 24 h at 4°C. After the incubation the product was centrifuged at 10,000 *g* for 15 min and the supernatant was used for incubation with sections (Eriksson et al., 1999). (3) Next we used OB tissues from non-infected TNFα knock out (KO) (Jackson Laboratories, strain name: B6.129S-*Tnf*^{tm1Gkl}/J, stock #: 005540) or IL1β KO mice on a C57BL/6 background (a gift from Dr Kerry O'Banion, University of Rochester, NY) to stain sections with DAB. (4) Next, Western blot analyses for TNFα and IL1β were performed as previously described (Szentirmai et al., 2007) using mouse OBs to demonstrate antibody recognition of the two forms (see below) of TNFα and IL1β. The primary antibodies used for western analyses were: a 1:150 dilution of goat anti-rat TNFα (R&D systems) or 1:1000 dilution of mouse anti-IL1β antibody

(Millipore) in 5% nonfat dry milk/Tween tris-buffered saline (TTBS) and a 1:4,000 dilution of horse anti-goat HRP conjugated secondary antibody (TNFα) or a 1:4,000 dilution goat anti-rabbit horseradish peroxidase (HRP) conjugated secondary antibody (IL1β). (5) Finally, in previous work using rats and a TNFα small interfering (si)RNA, we demonstrated that a TNFα siRNA reduced mRNA levels and TNFα-immunoreactivity in the brain using the same antibody that we used in the current experiments (Taishi et al., 2007).

Omission of the primary TNFα antibody eliminated the immunoreactivity in the OB sections (data not shown). Pre-absorption of the primary antibody with the recombinant TNFα protein, blocked the staining in both WT and KO mice (Figs. 1C and 1D for TNFα). TNFα immunoreactivity was observed in neuron-like cells in the OB of TNFα wild-type mice (WT) but not in the OB of the TNFα-KO mice (Figs. 1A and 1B for TNFα). Western blot analysis showed a 17 kD band for the recombinant protein and a 26 kD band in the OB protein extracts (data not shown); the molecular weight of membrane-associated TNFα is 26 kD (Solomon et al., 1999).

Omission of the primary IL1β antibody also eliminated immunoreactivity in OB sections (data not shown). After pre-absorption with the recombinant protein, IL1β immunoreactivity was greatly reduced but not completely blocked (Fig. 1C for IL1β). IHC for IL1β showed intensely stained IL-1β-IR cells in the EPL and GL (Fig. 1A for IL1β). These IL1β-IR cells were not observed in the EPL or GL of the OB from the IL1β KO mice (Fig. 1B for IL1β). Western blot analyses of OB protein extracts demonstrated the presence of a 17 kD band for the recombinant protein and a 37 kD band, which is the molecular weight of pro-IL1β (Deak et al., 2005) (data not shown). Pre-absorption treatment with the respective recombinant protein prior to Western blot completely eliminated the presence of these bands (data not shown). We also examined midbrain sections from TNFα and IL1β KO mice; these mice lacked TNFα or IL1β immunoreactivity using the procedures described herein (data not shown).

2.7. Image preparation

For DAB-stained sections, images in a Leica DMLB microscope were captured with a spot camera and associated software (Diagnostic Instruments Inc., Sterling Heights MI) before being transferred into Adobe Photoshop CS2 (Adobe Systems Inc., San Jose, CA). Adobe Photoshop was used only for brightness and contrast adjustments for photographs used in the quantitative analysis. For the fluorescent-antibody IHC, double-stained sections were photographed using the Spot camera with the light microscope as described above or using a confocal laser scanning microscope (Zeiss LSM-510, Oberkochen, Germany) equipped with an AxioCam HR digital camera (Zeiss). Confocal microscope pictures were taken using the Argon 488 nm laser for Alexa fluor 488 and the HeNe 543 nm laser for Alexa fluor 568. Single plane with full resolution was used for each fluorescence channel.

2.8. Quantitative analyses

Virus- and cytokine-IR cells were counted in printed digital images using transparent templates of the appropriate scale. The number of rostral OB IR-cells was determined using a transparent template with a rectangular box that measured 0.25 mm by 0.5 mm for photographs taken at 20X (TNFα–IR cells) or 0.20 mm by 0.22 mm for photographs taken at 40X (IL1β- and F4/80-IR cells) in 6 different fields. For mitral cell layer (ML) quantification, the rectangle was 0.1 mm by 0.5 mm for the 20X photographs and 0.04 mm by 0.20 mm for the 40X photographs. The total number of IR cells was averaged within the 6 different fields for each mouse in the OB. In the olfactory and central autonomic nervous systems, the number of IR-cells was determined using a rectangular box that measured 0.15 mm by 0.35 mm [the piriform cortex (Pir) and the olfactory tubercle (Tu)]; 0.15 mm by 0.075 mm (Arc), 0.3 mm by 0.3 mm (MPO) or a circle with a radius of 0.100 mm (BLA and CeA). In the Sctx, a rectangular box that

measured 0.5 mm by 0.225 mm was placed over photographs taken at 20 x in layers II–IV and layer V for both TNF and IL1β-IR cells. The number of sections analyzed for each mouse varied depending on the number available for each brain region. Normally three-six different fields were analyzed for each mouse. For all the analyzed regions an individual blinded to the experimental treatment completed the quantification. Means ± the standard error of the mean were calculated and then statistically analyzed using a paired Student's t-test. A p-value of 0.05 or less was considered statistically significant. Additionally, IR-cells were divided according to their morphology and size into two groups: glial cells [ramified cells between 5–15 microns in size that showed the immunoreactivity both in the cell body (< 5 microns) and in the ramifications] or neurons (non-ramified cells or cells with one or two branches between 10–30 microns in size that mainly showed immunoreactivity in the cell body) and then quantified as above.

3. Results

3.1. Immunoreactive cells in the OB of infected or control mice at 10 or 15 h PI

3.1.1. Influenza virus-IR cells within the OB—In mice inoculated with live virus, immunoreactivities for H1N1 and NP antigens were present mainly in the olfactory nerve (ON) layer and the glomerular layer (GL) of the OB both at 10 h and 15 h PI (Fig. 2). Viral antigen immunoreactivity was rarely detected in mice inoculated with heat-inactivated (boiled) PR8, as previously reported (Majde et al., 2007). The topographical distribution of the viral antigen-IR cells was characterized by a ventrolateral localization (Fig. 2A and B) close to the entry of the ON into the OB from the cribriform plate.

The viral protein-IR cells in the ON, the GL and, to a lesser extent, the external plexiform layer (EPL) (Fig 3B and C) resembled F4/80-IR cells with numerous processes and microglia-like morphology (Figs. 2C and 3A). We also found that viral antigen immunoreactivity was also present in a group of densely stained fusiform-like cells resembling olfactory ensheathing cells (OEC) in the ON (Au et al., 2002). These cells were located along the ON parallel to the nerve fibers (Fig. 4). No viral protein immunoreactivity was observed in neuron-like cells (see below).

3.1.2. F4/80-IR cells in the OB—In the OB, F4/80 immunoreactivity (Fig. 2C) was evident in numerous ramified cells with microglia-like morphology; these cells had a topographic distribution similar to viral antigen-IR cells (compare Fig. 2C to 2A and Fig. 3A to 3B and C). F4/80-IR cells were most densely distributed in the GL with occasional F4/80-stained cells also seen in the ON layer and the EPL (Fig. 2C). The morphology of the F4/80-IR cells in the GL was altered by the live PR8 infection; the processes were shorter, thicker and more densely stained with F4/80 antibody (Figs. 5B and 5D) in comparison with F4/80-stained cells in the GL from the mice inoculated with boiled virus (Figs. 5A and 5C). Further, the cell bodies of the F4/80-IR cells from the mice inoculated with live virus (Fig. 5B) appeared to be more densely stained relative to cell bodies in boiled-virus control cells. The F4/80-IR cells in the infected mouse OB were morphologically similar to activated microglia (Perry, 1994). The number of F4/80-IR cells in the GL was not statistically different at 10 h PI between mice that received boiled virus (5.8 ± 0.3) and mice that received live virus (6.7 ± 0.8, p=0.08). Similarly, at 15 h PI, there were no significant differences between the number of F4/80-IR cells in mice inoculated with live virus (17.4 ± 1.7) compared with mice inoculated with boiled virus (17.9 ± 2.0, p=0.78).

3.1.3. Co-localization of viral antigen with F4/80 staining—H1N1 viral antigen frequently co-localized with the macrophage marker F4/80 within microglia-like cells in the GL (Fig. 6A).

3.1.4. Co-localization of viral antigen with GFAP staining—GFAP-immunoreactivity was observed in multi-branched cells of about 15–20 microns in diameter. These cells were observed in the ON, GL and EPL, with the GL showing a more abundant population of the GFAP-IR cells. However, in double-labeled OB sections the GFAP-IR cells that co-localized with the anti-H1N1 antibodies were observed only in the GL (e.g., Fig. 6B). There were only a few double-labeled GFAP-H1N1-IR cells in the OB. This is in contrast with the relatively abundant double-labeled cells detected with the F4/80 and H1N1 antibodies in the same layer (Fig. 6A).

3.1.5. Co-localization of viral antigen with NeuN staining—NeuN-IR cells were found in both the GL and the EPL; however, not all cells with neuronal morphology in the analyzed regions showed NeuN-immunoreactivity. None of the NeuN-IR cells showed co-localization with the viral H1N1 antigen in any of the analyzed layers, though H1N1 staining was detected in adjacent microglia-like cells as mentioned in Sec. 2.6 (Fig. 6C).

3.1.6. Quantification of OB TNFα-IR cells in infected versus control mice at 10 or 15 h PI—A large number of TNFα-IR cells were observed in the GL, EPL and ML of the DAB-stained section. Absolute TNFα-IR cell numbers with statistical analysis are provided in Table 1. At 10 h PI there were no significant changes in the numbers of TNFα-IR cells in the rostral layers of the OB, but at 15 h PI, significant increases occurred in infected mice in the EPL and the ML, but not the GL, relative to the boiled virus controls.

The morphology of the TNFα-IR cells resembled neurons, i.e., the cells were between 10 to 30 μm in diameterwith a lightly stained rounded nucleus surrounded by more darkly stained cytoplasm (Fig. 7A and B). An apical dendrite was usually evident in the TNFα-IR cells in the EPL but not in the GL. TNFα-immunoreactivity was present in cell bodies as well as in fiber-like processes in the EPL. The morphology of the TNFα–IR cells was similar in live virus and control mice. Double labeling of the OB with a combination of anti-TNFα and anti-NeuN antibodies confirmed that TNRα-immunoreactivity was localized in the cytoplasm of neurons labeled with NeuN in the nucleus (Fig. 6D).

3.1.7. Quantification of OB IL1β-IR cells in infected versus control mice at 10 or 15 h PI—IL1β-IR cells were detected in the GL and the EPL. IL1β-IR cells morphologically resembled either neurons (as described above for TNFα-IR cells) or glia [i.e., ramified cells between 5–15 microns in diameter that showed several darkly-stained projections and a small dark nucleus (Fig. 8)]. The number of IL1β-IR glial-like cells within the various OB layers was similar in live virus and control groups and consequently significant differences between the two groups were not found (data not shown). Absolute numbers of IL1β-IR neuron-like cells with statistical analysis are provided in Table 2. The number of IL1β-IR neuron-like cells was not significantly increased at 10 h PI in the rostral OB but was significantly increased in the EPL, but not the GL or the ML, at 15 h PI (Table 2).

Adjacent sections processed for double labeling with the IL1β antibody and cell markers confirmed that IL1β-immunoreactivity co-localized with NeuN (Fig. 6E) in the GL and EPL, and with GFAP (Fig. 6F) or F4/80 (Fig. 6G) in the GL.

3.2.1. Viral antigen immunoreactivity in the midbrain—No H1N1 or NP viral antigen immunoreactivity was found in the Pir, Tu, the amygdale, Sctx, MPO or Arc either at 10 h or at 15 h PI.

3.2.2. Quantification of midbrain TNFα-IR cells in infected versus control mice at 10 or 15 h PI—Absolute numbers and statistical analysis of TNFα-IR cells in the midbrain regions examined are provided in Table 1. At 10 h PI there were no significant changes in the

number of TNFα-IR cells in the olfactory cortex, Sctx layers or central autonomic regions examined, but at 15 h PI, significant increases in TNFα-IR cell numbers occurred in infected mice relative to boiled controls in the Pir, Tu, and CeA but not the BLA, Sctx layers or arcuate. TNFα immunoreactivity was mainly observed in layer II of the Pir and the dense cell layer (DCL) of the Tu (Fig. 9, left side).

3.2.3. Quantification of midbrain IL1β-IR cells in infected versus control mice at 10 or 15 h PI—IL1β-IR cells in the midbrain morphologically resembled neurons but not glial cells. Absolute numbers of IL1β-IR neuron-like cells with statistical analysis are provided in Table 2. The number of IL1β-IR neuron-like cells in infected mice was not significantly increased at 10 h PI from control values (derived from mice infected with boiled virus) in any midbrain region examined. However, at 15 h PI the number of neuron-like cell staining for IL1β was significantly increased in the Pir, Tu, CeA, MPO and Arc, but not the BLA or Sctx layers, of infected mice compared to boiled virus controls (Table 2). IL1β immunoreactivity was mainly observed in layer II of the Pir and the DCL of the Tu (Fig. 9, right side).

3.2.4. Cytokine association with midbrain neurons using double labeling—Both TNFα and IL1β immunoreactivity co-localized with NeuN in the examined areas. An example of co-localization in the CeA is shown for TNFα and NeuN (Fig. 10A) and IL-1β and NeuN (Fig. 10B).

4. Discussion

In the GL and the EPL, glial cells positive for F4/80- or GFAP-immunoreactivity harbor influenza antigens after IN infection with PR8 influenza virus. The majority of these cells appeared morphologically similar to microglia, though microglia cannot be distinguished from dendritic cells by morphology or F4/80 staining and are found in the same region of the OB (Bulloch et al., 2008). Microglial cells are considered to be immune-effector cells in the brain (Guillemin and Brew, 2003) having the capacity to clear viruses and virus-infected cells (Hauwel et al., 2005). Additionally, we found that viral protein-immunoreactivity co-localized with the astrocyte marker GFAP, suggesting that these cells also take up the virus after its entrance into the GL. PR8 influenza is known to persistently infect mouse astrocytes *in vitro* with minimal release of infectious virus (Bradshaw, et al., 1989). Both microglia and astrocytes in mice bear the receptors for human and avian influenza viruses (Wang, et al., 2008) and will support replication of non-mouse-adapted influenza strains *in vitro*. Whether these glial cells support influenza replication *in vivo* is not known.

F4/80-IR OB cells in mice receiving live virus were morphologically distinct from those F4/80-IR cells of mice inoculated with boiled virus. The thicker and shorter processes, as well as the darkly stained cell bodies, suggest that the cells are activated. After viral or bacterial infections microglia rapidly undergo activation as indicated by changes in their morphology (Deng et al., 2006) similar to those reported here, and express phagocytic markers (Kumaraswamy et al., 2006; Lehnardt et al., 2006; Ghoshal et al., 2007; Lemstra et al., 2007). That the number of F4/80-IR cells did not significantly change after infection with live virus either at 10 h or 15 h PI, suggests that the F4/80-IR cells were resident microglia or dendritic cells, not macrophages migrating from the blood (Perry et al., 1985; Deshpande et al., 2007).

We failed to demonstrate the co-localization of viral proteins within neurons using the neuronal marker NeuN. However, recent studies (Kumar and Buckmaster, 2007; Parrish-Aungst et al., 2007) indicate that the neuronal marker NeuN does not label all OB neurons, leaving open the possibility that *in vivo* neurons could take up viral protein and/or virus. However, there is no evidence indicating that the PR8 strain of influenza is able to replicate in neurons (Bradshaw, et al., 1989).

In the ON we observed that viral proteins were present in large fusiform cells resembling olfactory ensheathing cells (OECs) (Au et al., 2002). OECs wrap the axons of the olfactory receptor neurons and together with ON fibroblasts form channels capable of transporting 100 nm mineral particles to the OB glomeruli (Li et al., 2005; Vincent et al., 2005). If influenza virus enters OEC channels, the OECs are phagocytic and endocytotic (Leung et al, 2008) and could possibly take up virions from within these channels. Full or partial replication of the virus within the OECs would then lead to the expression of viral antigens and binding of influenza antibodies, accounting for our observations. Direct evidence for this hypothesis is lacking, but we speculate that OEC channels are one of several possible pathways that may be involved in the transport of the influenza virus to the OB (Majde et al., 2007).

The increase in the number of cells expressing TNFα and IL1β proteins in the OB in response to live virus extends our previous observations of virus-enhanced TNFα and IL1β mRNAs in the OB at 15 h PI (Majde et al., 2007). The differences in distribution of cytokine-IR cells in the GL, EPL and the ML may be a manifestation of sequential events within the OB, including the dynamics of virus distribution or that of its dsRNA replication intermediates (Majde et al., 1998).

The second major finding described herein was the presence of enhanced cytokine–IR cell numbers after viral challenge in brain regions such as the olfactory cortex and central autonomic system. Though cytokines are not normally recognized as neuronal components, substantial evidence demonstrates that neurons produce pro-inflammatory cytokines in response to pathological conditions and activate microglia to become antigen-presenting cells (Liu et al., 1994; Ohtori et al., 2004; Yang et al., 2004; Figiel and Dzwonek, 2007). Furthermore, our findings of TNFα- and IL1β-immunoreactivity in neurons confirm prior results demonstrating neuronal expression of these cytokines (Breder et al., 1993; Breder et al., 1994; Ignatowski et al., 1997; Lim and Brunjes, 1999; Gao et al., 2000; Acarin et al., 2000; Ji et al., 2005; Figiel and Dzwonek, 2007; Mao et al., 2006; Kwon et al., 2008). Our methods do not distinguish between cytokines synthesized by neurons and uptake of glial cytokines by nearby neurons

Viruses transported via the ON to the OB have the potential to signal caudal regions of the brain via glial products or activated neurons, or both, even though the viruses may not invade the brain further than the GL. In the GL, olfactory receptor neurons synapse with dendrites of second order neurons such as tufted and mitral cells (Kinoshita et al., 2002). The axons of OB tufted and mitral cells project to different brain regions including the Pir and the Tu, which are considered components of the olfactory cortex, (Josephson et al., 1997; Haberly, 2001; Suzuki and Bekkers, 2007). Projections from the OB also reach the amygdala at the anterior cortical nucleus and the posterolateral cortical amygdala (Price, 2003; Ubeda-Bañon et al., 2007). In addition, the BLA and CeA receive indirect connections from the OB through the Pir and through the anterior and posterolateral amygdala (Johnson et al., 2000; LeDoux, 2007). Bilateral lesions of the CeA attenuate herpes simplex virus-1-induced fever and increased locomotor activity in rats (Weidenfeld et al., 2005). Furthermore, after systemic injections with LPS (Konsman et al., 1999) or IL1β (Day et al., 1999), c-fos mRNA and protein expression increase in the CeA, indicating activation in response to antigen-induced stimulation (Sagar et al., 1995). These results suggest a role for the CeA in the regulation of the APR (Weidenfeld et al., 2005). Our results are consistent with this idea because we found that the number of TNFα and IL1β-IR cells increased in the CeA in response to viral challenge.

The Pir is also indirectly connected to the hypothalamic arcuate nucleus (Arc) (Chiba and Murata, 1985; Lin and York, 2004; Price et al., 1991; Price, 2003). The Arc is another area implicated in the regulation of the APR, including hypothermia and anorexia responses (Jolicoeur, et al., 1995). Pro-inflammatory stimuli, such as IL1β or LPS or *Staphylococcus* enterotoxin, given systemically enhance the expression of the neuronal activity marker c-Fos

in the Arc (Bluthe et al., 2000; Reyes and Sawchenko, 2002; Scarlett et al., 2007; Rossi-George et al., 2005). Our results are consistent with those findings to the extent that after viral challenge Arc IL1β-positive neurons increase (see discussion below). The Arc is close to the median eminence, a circumventricular organ lacking the blood-brain-barrier. It is thus possible that the enhanced Arc IL1β may result from signals of blood origin. After influenza PR8 challenge, virus is sporadically detected in blood (Mori et al., 1995; Majde et al., 2007). Another possibility is that cytokines of peripheral origin (e.g. lungs) signal the hypothalamus via afferent vagal fibers to the nucleus tractus solitarius in the brainstem and from there via neurons that project to the Arc (Hansen et al., 1998; Goehler et al., 2000; Kubota et al., 2001; Matsuda et al., 2004; Wieczorek et al., 2005) because vagotomy blocks intraperitoneal IL1β-induced up regulation of hypothalamic IL1β transcripts (Hansen et al., 1998).

The OB is also indirectly connected to the MPO (Shipley et al., 2004), another brain region implicated in body temperature regulation (Szymusiak and Satinoff, 1982). Parts of the amygdala that receive olfactory input project to the medial and anterior hypothalamus, which includes the MPO (Shipley et al., 2004). The MPO has been implicated in the actions of IL1β on body temperature in rats (Sellami and de Beaurepaire, 1995). Therefore, our results showing an increase in the number of IL1β-IR cells in the MPO supports the role of these cells in the hypothermic response to the viral infection.

The lack of virus immunoreactivity in the different regions of the midbrain suggests that the observed increases in midbrain cytokines are not directly induced by local virus. It is well-known that TNFα and IL1β induce each other and their own production (Vitkovic et al., 2000; Silverman et al., 2005). Cytokines released into the extracellular space, such as TNFα and IL1β, likely stimulate nearby neuronal TNFα and IL1β production.

The increases in cytokine expressing neurons in the hypothalamus reported here may be related to body temperature, food intake, sleep responses and other characteristic changes in sickness behavior. While infections are generally associated with fever, and mice can generate a fever with certain stimuli (Kozak et al., 1995), influenza in mice is marked by a stereotypic hypothermia response, that like fever, seems to be regulated (Conn et al., 1995; Fang et al., 1995; Toth et al., 1995; Romanovsky et al., 2005). Further, mice become anorexic after influenza challenge and can lose up to 20% of their body weight before death or recovery (Conn et al., 1995). Mice also sleep substantially more for days after influenza challenge (Fang et al., 1995; Toth et al., 1995). Both TNFα and IL1β injected intracerebroventricularly cause anorexia (Plata-Salaman et al., 1988) and enhance sleep (Krueger et al., 1984). These responses are likely brought about via multiple actions by IL1β and TNFα. For example, IL1β inhibits neuropeptide Y (NPY)-induced feeding and suppresses arcuate NPY levels (Gayle et al., 1997). Neuropeptide Y inhibits sleep (Szentirmai et al., 2006). Regardless of the mechanisms of influenza-induced changes in sickness behavior, such responses appear protective (e.g., Klein et al., 1992).

In conclusion, the results presented here indicate that PR8 influenza virus localizes to glia in the GL of the OB leading to the production of pro-inflammatory cytokines in the OB and in increased numbers of neurons within different regions of the brain; i.e., olfactory cortex (Pir and Tu), a region of the amygdala with projections from the olfactory cortex (the CeA) and temperature-regulating regions of the hypothalamus (the MPO and Arc) at 15 h. The enhanced neuronal expression of cytokines is evident when the animals are responding to the viral challenge (15 h) but not at 10 h PI prior to illness onset.

Acknowledgments

We would like to acknowledge Andrea Bouchet for her technical assistance and Bryan Slinker for his advice on statistical analyses. This work was supported by the Institute of Child Health and Development NIH Grant No.

HD36520 and the National Institute of Neurological Disorders and Stroke Grant Nos. NS25378 and NS31453. Dr. Leyva-Grado was supported by the Direccion General de Apoyo al Personal Academico of the National Autonomous University of Mexico.

References

Acarin L, González B, Castellano B. Neuronal, astroglial and microglial cytokine expression after an excitotoxic lesion in the immature rat brain. Eur J Neurosci 2000;12:3505–3520. [PubMed: 11029620]

Au WW, Treloar HB, Greer CA. Sublaminar organization of the mouse olfactory bulb nerve layer. J Comp Neurol 2002;446:68–80. [PubMed: 11920721]

Barbe ME, Barr AE, Gorzelany I, Amin M, Gaughan JP, Safadi FF. Chronic repetitive reaching and grasping results in decreased motor performance and widespread tissue responses in a rat model of MSD. J Orthop Res 2003;21:167–176. [PubMed: 12507595]

Ben Hur T, Rosenthal J, Itzik A, Weidenfeld J. Adrenocortical activation by herpes virus: involvement of IL-1 beta and central noradrenergic system. Neuroreport 1996;7:927–931. [PubMed: 8724676]

Bluthé RM, Layé S, Michaud B, Combe C, Dantzer R, Parnet P. Role of interleukin-1beta and tumour necrosis factor-alpha in lipopolysaccharide-induced sickness behaviour: a study with interleukin-1 type I receptor-deficient mice. Eur J Neurosci 2000;12:4447–4456. [PubMed: 11122355]

Bradshaw GL, Schlesinger RW, Schwartz CD. Effects of cell differentiation on replication of A/WS/33, WSN, and A/PR/8/34 influenza viruses in mouse brain cell cultures: biological and immunological characterization of products. J Virol 1989;63:1704–1714. [PubMed: 2648025]

Breder CD, Tsujimoto M, Terano Y, Scott DW, Saper CD. Distribution and characterization of tumor necrosis factor-alpha-like immunoreactivity in the murine central nervous system. J Comp Neurol 1993;337:543–567. [PubMed: 8288770]

Breder CD, Hazuka C, Ghayur T, Klug C, Huginin M, Yasuda K, Teng M, Saper CB. Regional induction of tumor necrosis factor alpha expression in the mouse brain after systemic lipopolysaccharide administration. Proc Natl Acad Sci 1994;91:11393–11397. [PubMed: 7972071]

Bulloch K, Miller MM, Gal-Toth J, Milner TA, Gottfried-Blackmore A, Waters EM, Kaunzner UW, Liu K, Lindquist R, Nussenzweig MC, Steinman RM, McEwen BS. CD11c/EYFP transgene illuminates a discrete network of dendritic cells within the embryonic, neonatal, adult and injured mouse brain. J Comp Neurol 2008;508:687–710. [PubMed: 18386786]

Chen L, Duricka D, Nelson S, Mukherjee S, Bohnet SG, Taishi P, Majde JA, Krueger JM. Influenza virus-induced sleep responses in mice with targeted disruptions in neuronal or inducible nitric oxide synthases. J Appl Physiol 2004;97:17–28. [PubMed: 15220315]

Chiba T, Murata Y. Afferent and efferent connections of the medial preoptic area in the rat: a WGA-HRP study. Brain Res Bull 1985;14:261–272. [PubMed: 3995367]

Churchill L, Yasuda K, Yasuda T, Blindheim KA, Falter M, Garcia-Garcia F, Krueger JM. Unilateral cortical application of tumor necrosis factor-α induces asymmetry in Fos- and interleukin-1β-immunoreactive cells within the corticothalamic projection. Brain Res 2005;1055:15–24. [PubMed: 16098952]

Conn CA, McClellan JL, Maassab HF, Smitka CW, Majde JA, Kluger MJ. Cytokines and the acute phase response to influenza virus in mice. Am J Physiol 1995;268:R78–R84. [PubMed: 7530928]

Day HE, Curran EJ, Watson SJ Jr, Akil H. Distinct neurochemical populations in the rat central nucleus of the amygdala and bed nucleus of the stria terminalis: evidence for their selective activation by interleukin-1beta. J Comp Neurol 1999;413:113–128. [PubMed: 10464374]

Deak T, Bordner KA, McElderry NK, Barnum CJ, Blandino P Jr, Deak MM, Tammariello SP. Stress-induced increases in hypothalamic IL-1: a systematic analysis of multiple stressor paradigms. Brain Res Bull 2005;30:541–556. [PubMed: 15639551]

Deng XH, Bertini G, Xu YZ, Yan Z, Bentivoglio M. Cytokine-induced activation of glial cells in the mouse brain is enhanced at an advanced age. Neuroscience 2006;141:645–661. [PubMed: 16730918]

Deshpande P, King II, Segal BM. Cutting Edge: CNS CD11c+ cells from mice with encephalomyelitis polarize Th17 cells and support CD25+CD4+ T cell-mediated immunosuppression, suggesting dual roles in the disease process. J Immunol 2007;178:6695–6699. [PubMed: 17513712]

Eriksson C, Van Dam AM, Lucassen PJ, Bol JG, Winblad B, Schultzberg M. Immunohistochemical localization of interleukin-1beta, interleukin-1 receptor antagonist and interleukin-1beta converting

enzyme/caspase-1 in the rat brain after peripheral administration of kainic acid. Neuroscience 1999;93:915–930. [PubMed: 10473257]

Fang J, Sanborn CK, Renegar KB, Majde JA, Krueger JM. Influenza viral infections enhance sleep in mice. Proc Soc Exp Biol Med 1995;210:242–252. [PubMed: 8539262]

Figiel I, Dzwonek K. TNFalpha and TNF receptor 1 expression in the mixed neuronal-glial cultures of hippocampal dentate gyrus exposed to glutamate or trimethyltin. Brain Res 2007;1131:17–28. [PubMed: 17161388]

Frenois F, Moreau M, O'Connor J, Lawson M, Micon C, Lestage J, Kelley KW, Dantzer R, Castanon N. Lipopolysaccharide induces delayed FosB/DeltaFosB immunostaining within the mouse extended amygdala, hippocampus and hypothalamus, that parallel the expression of depressive-like behavior. Psychoneuroendocrinology 2007;32:516–531. [PubMed: 17482371]

Gao Y, Ng YK, Lin JY, Ling EA. Expression of immunoregulatory cytokines in neurons of the lateral hypothalamic area and amygdaloid nuclear complex of rats immunized against human IgG. Brain Res 2000;859:364–368. [PubMed: 10719087]

Gayle D, Ilyin SE, Plata-Salaman CR. Central nervous system IL-1[beta] system and neuropeptide Y mRNAs during IL-1[beta]-induced anorexia in rats. Brain Res Bull 1997;44:311–317. [PubMed: 9323447]

Ghoshal A, Das S, Ghosh S, Mishra MK, Sharma V, Koh P, Sen E, Basu A. Proinflammatory mediators released by activated microglia induces neuronal death in Japanese encephalitis. Glia 2007;55:483–496. [PubMed: 17203475]

Goehler LE, Gaykema RP, Hansen MK, Anderson K, Maier SF, Watkins LR. Vagal immune-to-brain communication: a visceral chemosensory pathway. Auton Neurosci 2000;85:49–59. [PubMed: 11189026]

Guillemin GJ, Brew BJ. Microglia, macrophages, perivascular macrophages and pericytes: a review of function and identification. J Leukoc Biol 2003;75:388–397. [PubMed: 14612429]

Haberly L. Parallel-distributed processing in olfactory cortex: new insights from morphological and physiological analysis of neuronal circuitry. Chem Senses 2001;26:551–576. [PubMed: 11418502]

Hansen MK, Taishi P, Chen Z, Krueger JM. Vagotomy blocks the induction of interleukin-1beta (IL-1beta) mRNA in the brain of rats in response to systemic IL-1beta. J Neurosci 1998;18:2247–2253. [PubMed: 9482809]

Hauwel M, Furon E, Canova C, Griffiths M, Neal J, Gasque P. Innate (inherent) control of brain infection, brain inflammation and brain repair: the role of microglia, astrocytes, "protective" glial stem cells and stromal ependymal cells. Brain Res Rev 2005;48:220–233. [PubMed: 15850661]

Hennet T, Ziltener HJ, Frei K, Peterhans E. A kinetic study of immune mediators in the lungs of mice infected with influenza A virus. J Immunol 1992;149:932–939. [PubMed: 1321855]

Ignatowski TA, Noble BK, Wright JR, Gorfien JL, Heffner RR, Spengler RN. Neuronal-associated tumor necrosis factor (TNF alpha): its role in noradrenergic functioning and modification of its expression following antidepressant drug administration. J Neuroimmunol 1997;79:84–90. [PubMed: 9357451]

Iwasaki T, Itamura S, Nishimura H, Sato Y, Tashiro M, Hashikawa T, Kurata T. Productive infection in the murine central nervous system with avian influenza virus (H5N1) after intranasal inoculation. Acta Neuropathol 2004;108:485–492. [PubMed: 15480712]

Ji JF, Dheen ST, Kumar SD, He BP, Tay SS. Expressions of cytokines and chemokines in the dorsal motor nucleus of the vagus nerve after right vagotomy. Mol Brain Res 2005;142:47–57. [PubMed: 16260063]

Johnson DM, Illig KR, Behan M, Haberly LB. New features in connectivity in piriform cortex visualized by intracellular injection of pyramidal cells suggest that "primary" olfactory cortex function like "association" cortex in other sensory systems. J Neurosci 2000;20:6974–6982. [PubMed: 10995842]

Jolicoeur FB, Bouali SM, Fournier A, St-Pierre S. Mapping of hypothalamic sites involved in the effects of NPY on body temperature and food intake. Brain Res Bull 1995;36:125–129. [PubMed: 7895089]

Josephson E, Padgett ML, Buxton DF. The lateral and medial compartments of the olfactory tubercle and their relation to olfactory-related input as determined by artificial neural network. Brain Res 1997;744:253–271. [PubMed: 9027385]

Kinoshita N, Mizuno T, Yoshihara Y. Adenovirus-mediated WGA gene delivery for transsynaptic labeling of mouse olfactory pathways. Chem Senses 2002;27:215–223. [PubMed: 11923184]

Klein MS, Conn CA, Kluger MJ. Behavioral thermoregulation in mice inoculated with influenza virus. Physiol Behav 1992;52:1133–1139. [PubMed: 1484872]

Konsman JP, Kelley K, Dantzer R. Temporal and spatial relationships between lipopolysaccharide-induced expression of Fos, interleukin-1beta and inducible nitric oxide synthase in rat brain. Neuroscience 1999;89:535–548. [PubMed: 10077334]

Kozak W, Zheng H, Conn CA, Soszynski D, Van der Ploeg LHT, Kluger MJ. Thermal and behavioral effects of lipopolysaccharide and influenza in interleukin-1β deficient mice. Am J Physiol 1995;269:R969–R977. [PubMed: 7503324]

Krueger JM, Walter J, Dinarello CA, Wolff SM, Chedid L. Sleep-promoting effects of endogenous pyrogen (interleukin-1). Am J Physiol 1984;246:R994–R999. [PubMed: 6611091]

Kubota T, Fang J, Guan Z, Brown RA, Krueger JM. Vagotomy attenuates tumor necrosis factor-alpha-induced sleep and EEG delta-activity in rats. Am J Physiol Regul Integr Comp Physiol 2001;280:R1213–R1220. [PubMed: 11247847]

Kumar SS, Buckmaster PS. Neuron-specific nuclear antigen NeuN is not detectable in gerbil substantia nigra pars reticulata. Brain Res 2007;1142:54–60. [PubMed: 17291468]

Kumaraswamy GK, Fu MM, Docherty JJ. Innate and adaptive host response during the initial phase of herpes simplex virus encephalitis in the neonatal mouse. J Neurovirol 2006;12:365–374. [PubMed: 17065129]

Kwon MS, Seo YJ, Lee JK, Lee HK, Jung JS, Jang JE, Park SH, Suh HW. The repeated immobilization stress increases IL-1beta immunoreactivities in only neuron, but not astrocyte or microglia in hippocampal CA1 region, striatum and paraventricular nucleus. Neurosci Lett 2008;430:258–263. [PubMed: 18061345]

LeDoux J. The amygdala. Current Biology 2007;17:R868–R874. [PubMed: 17956742]

Lehnardt S, Henneke P, Lien E, Kasper DL, Volpe JJ, Bechmann I, Nitsch R, Weber JR, Golenbock DT, Vartanian T. A mechanism for neurodegeneration induced by group B streptococci through activation of the TLR2/MyD88 pathway in microglia. J Immunol 2006;177:583–592. [PubMed: 16785556]

Lemstra AW, Groen in't Woud JC, Hoozemans JJ, van Haastert ES, Rozemuller AJ, Eikelenboom P, van Gool WA. Microglia activation in sepsis: a case-control study. J Neuroinflammation 2007;4:4–12. [PubMed: 17224051]

Leung JY, Chapman JA, Harris JA, Hale D, Chung RS, West AK, Chuah MI. Olfactory ensheathing cells are attracted to, and can endocytose, bacteria. Cell Mol Life Sci 2008;65:2732–2739. [PubMed: 18604629]

Li Y, Field PM, Raisman G. Olfactory ensheathing cells and olfactory nerve fibroblasts maintain continuous open channels for regrowth of olfactory nerve fibers. Glia 2005;52:245–251. [PubMed: 15968636]

Lim JH, Brunjes PC. Activity-dependent regulation of interleukin-1 beta immunoreactivity in the developing rat olfactory bulb. Neuroscience 1999;93:371–374. [PubMed: 10430500]

Lin L, York DA. Amygdala enterostatin induces c-Fos expression in regions of hypothalamus that innervate the PVN. Brain Res 2004;1020:147–153. [PubMed: 15312796]

Liu T, Clark RK, McDonnell PC, Young PR, White RF, Barone FC, Feuerstein GZ. Tumor necrosis factor-alpha expression in ischemic neurons. Stroke 1994;25:1481–1488. [PubMed: 8023366]

Majde JA, Guha-Thakurta N, Chen Z, Bredow S, Krueger JM. Spontaneous release of stable viral double-stranded RNA into the extracellular medium by influenza virus-infected MDCK epithelial cells: implications for the viral acute phase response. Arch Virol 1998;143:2371–2380. [PubMed: 9930193]

Majde JA, Bohnet SG, Ellis GA, Churchill L, Leyva-Grado VH, Wu M, Szentirmai E, Rehman A, Krueger JM. Detection of mouse-adapted human influenza viruses in the olfactory bulbs of mice within hours after intranasal inoculation. J Neurovirol 2007;13:399–409. [PubMed: 17994424]

Mao M, Hua Y, Jiang X, Li L, Zhang L, Mu D. Expression of tumor necrosis factor alpha and neuronal apoptosis in the developing rat brain after neonatal stroke. Neurosci Lett 2006;403:227–232. [PubMed: 16797840]

Matsuda K, Park CH, Sunden Y, Kimura T, Ochiai K, Kida H, Umemura T. The vagus nerve is one route of transneural invasion for intranasally inoculated influenza a virus in mice. Vet Pathol 2004;41:101–107. [PubMed: 15017022]

McQuillin J, Madeley CR, Kendal AP. Monoclonal antibodies for the rapid diagnosis of influenza A and B virus infections by immunofluorescence. Lancet 1985;2:911–914. [PubMed: 2865418]

Mori I, Komatsu T, Takeuchi K, Nakakuki K, Sudo M, Kimura Y. Viremia induced by influenza virus. Microbiol Pathog 1995;19:237–244.

Ohtori S, Takahashi K, Moriya H, Myers RR. TNF-alpha and TNF- alpha receptor type 1 upregulation in glia and neurons after peripheral nerve injury: studies in murine DRG and spinal cord. Spine 2004;29:1082–1088. [PubMed: 15131433]

Parrish-Aungst S, Shipley MT, Erdelyi F, Szabo G, Puche AC. Quantitative analysis of neuronal diversity in the mouse olfactory bulb. J Comp Neurol 2007;501:825–836. [PubMed: 17311323]

Perry VH, Hume DA, Gordon S. Immunohistochemical localization of macrophages and microglia in the adult and developing mouse brain. Neuroscience 1985;15:313–326. [PubMed: 3895031]

Perry VH. Modulation of microglia phenotype. Neuropathol Appl Neurobiol 1994;20:177. [PubMed: 8072647]

Plata-Salaman CR, Oomura Y, Kai Y. Tumor necrosis factor and interleukin-1β: Suppression of food intake by direct action in the central nervous system. Brain Res 1988;448:106–114. [PubMed: 3260533]

Price JL, Slotnick BM, Revial MF. Olfactory projections to the hypothalamus. J Comp Neurol 1991;306:447–461. [PubMed: 1713925]

Price JL. Comparative aspects of amygdala connectivity. Ann NY Acad Sci 2003;985:50–58. [PubMed: 12724147]

Reyes TM, Sawchenko PE. Involvement of the arcuate nucleus of the hypothalamus in interleukin-1-induced anorexia. J Neurosci 2002;22:5091–5099. [PubMed: 12077204]

Romanovsky AA, Almeida MC, Aronoff DM, Ivanov AI, Konsman JP, Steiner AA, Turek VF. Fever and hypothermia in systemic inflammation: recent discoveries and revisions. Front Biosci 2005;10:193–216.

Rossi-George A, Urbach D, Colas D, Goldfarb Y, Kusnecov AW. Neuronal, endocrine, and anorexic responses to the T-cell superantigen staphylococcal enterotoxin A: dependence on tumor necrosis factor-alpha. J Neurosci 2005;25:5314–5322. [PubMed: 15930379]

Sagar SM, Price KJ, Kasting NW, Sharp FR. Anatomic patterns of Fos immunostaining in rat brain following systemic endotoxin administration. Brain Res Bull 1995;36:381–392. [PubMed: 7712198]

Scarlett JM, Jobst EE, Enriori PJ, Bowe DD, Batra AK, Grant WF, Cowley MA, Marks DL. Regulation of central melanocortin signaling by interleukin-1 beta. Endocrinology 2007;148:4217–4225. [PubMed: 17525125]

Schlesinger RW. Incomplete growth cycle of influenza virus in mouse brain. Proc Soc Exp Biol Med 1950;74:541–548. [PubMed: 15440881]

Schlesinger RW, Husak PJ, Bradshaw GL, Panayotov PP. Mechanisms in natural and experimental neuropathogenicity of influenza viruses: evidence and speculation. Adv Virus Res 1998;50:289–379. [PubMed: 9521002]

Sellami S, de Beaurepaire R. Hypothalamic and thalamic sites of action of interleukin-1 beta on food intake, body temperature and pain sensitivity in the rat. Brain Res 1995;694:69–77. [PubMed: 8974666]

Shipley, MT.; Ennis, M.; Puche, AC. Olfactory System. In: Paxinos, G., editor. The Rat Nervous System, Chapter 25. 2004. p. 923-964.

Silverman MN, Pearce BD, Biron CA, Miller AH. Immune modulation of the hypothalamic-pituitary-adrenal (HPA) axis during viral infection. Viral Immunol 2005;18:41–78. [PubMed: 15802953]

Solomon KA, Pesti N, Wu G, Newton RC. Cutting edge: a dominant negative form of TNF-alpha converting enzyme inhibits proTNF and TNFRII secretion. J Immunol 1999;163:4105–4108. [PubMed: 10510344]

Stangel M, Compston A. Polyclonal immunoglobulins (IVIg) modulate nitric oxide production and microglial functions in vitro via Fc receptors. J Neuroimmunol 2001;112:63–71. [PubMed: 11108934]

Stichel CC, Luebbert H. Inflammatory processes in the aging mouse brain: participation of dendritic cells and T-cells. Neurobiol Aging 2007;28:1507–1521. [PubMed: 16959379]

Suzuki N, Bekkers JM. Inhibitory interneurons in the piriform cortex. Clin Exp Pharmacol Physiol 2007;34:1064–1069. [PubMed: 17714095]

Szentirmai E, Krueger JM. Central administration of neuropeptide Y induces wakefulness in rats. Am J Physiol Regul Integr Comp Physiol 2006;291:R473–R480. [PubMed: 16914434]

Szentirmai E, Kapás L, Sun Y, Smith RG, Krueger JM. Spontaneous sleep and homeostatic sleep regulation in ghrelin knockout mice. Am J Physiol Regul Integr Comp Physiol 2007;293:R510–R517. [PubMed: 17409264]

Szymusiak R, Satinoff E. Acute thermoregulatory effects of unilateral electrolytic lesions of the medial and lateral preoptic area in rats. Physiol Behav 1982;28:161–170. [PubMed: 7079312]

Taishi P, Churchill L, Wang M, Kay D, Davis CJ, Guan X, De A, Yasuda T, Liao F, Krueger JM. TNF alpha siRNA reduces brain TNF and EEG delta wave activity in rats. Brain Res 2007;1156:125–132. [PubMed: 17531209]

Toth LA, Rehg JE, Webster RG. Strain differences in sleep and other pathophysiological sequelae of influenza virus infection in naive and immunized mice. J Neuroimmunol 1995;58:89–99. [PubMed: 7730450]

Ubeda-Bañon I, Novejarque A, Mohedano-Moriano A, Pro-Sistiaga P, de la Rosa-Prieto C, Insausti R, Martinez-Garcia F, Lanuza E, Martinez-Marcos A. Projections from the posterolateral olfactory amygdala to the ventral striatum: neural basis for reinforcing properties of chemical stimuli. BMC Neurosci 2007;8:103–113. [PubMed: 18047654]

Ubink R, Halasz N, Zhang X, Dagerlind A, Hokfelt T. Neuropeptide tyrosine is expressed in ensheathing cells around the olfactory nerves in the rat olfactory bulb. Neuroscience 1994;60:709–726. [PubMed: 7936197]

Vacheron F, Rudent A, Perin S, Labarre C, Quero AM, Guenounou M. Production of interleukin 1 and tumour necrosis factor activities in bronchoalveolar washings following infection of mice by influenza virus. J Gen Virol 1990;71:477–479. [PubMed: 2137872]

Vincent AJ, West AK, Chuah ML. Morphological and functional plasticity of olfactory ensheathing cells. J Neurocytol 2005;34:65–80. [PubMed: 16374710]

Vitkovic L, Konsman JP, Bockaert J, Dantzer R, Homburger V, Jacque C. Cytokine signals propagate through the brain. Mol Psych 2000;5:604–615.

Walls HH, Harmon MW, Slagle JJ, Stocksdale C, Kendall AP. Characterization and evaluation of monoclonal antibodies developed for typing influenza A and influenza B viruses. J Clin Microbiol 1986;23:240–245. [PubMed: 3517049]

Wang G, Zhang J, Li W, Xin G, Su Y, Gao Y, Zhang H, Lin G, Jiao X, Li K. Apoptosis and proinflammatory cytokine responses of primary mouse microglia and astrocytes induced by human H1N1 and avian H5N1 influenza viruses. Cell Mol Immunol 2008;5:113–120. [PubMed: 18445341]

Wieczorek M, Swiergiel A, Pournajafi-Nazarloo H, Dunn AJ. Physiological and behavioral responses to interleukin-1beta and LPS in vagotomized mice. Physiol Behav 2005;85:500–511. [PubMed: 15996692]

Weidenfeld J, Itzik A, Goshen I, Yirmiya R, Ben-Hur T. Role of the central amygdala in modulating the pituitary-adrenocortical and clinical responses in experimental herpes simplex virus-1 encephalitis. Neuroendocrinology 2005;81:267–272. [PubMed: 16131813]

Wilkinson J, Radkowski M, Laskus T. Hepatitis C virus neuroinvasion: identification of infected cells. J Virol 2009;83:1312–1319. [PubMed: 19019968]

Xu Y, Day TA, Buller KM. The central amygdala modulates hypothalamic-pituitary-adrenal axis responses to systemic interleukin-1beta administration. Neuroscience 1999;94:175–183. [PubMed: 10613507]

Yang L, Blumbergs PC, Jones NR, Manavis J, Sarvestani GT, Ghabriel MN. Early expression and cellular localization of proinflammatory cytokines interleukin-1beta, interleukin-6, and tumor necrosis factor-alpha in human traumatic spinal cord injury. Spine 2004;29:966–971. [PubMed: 15105666]

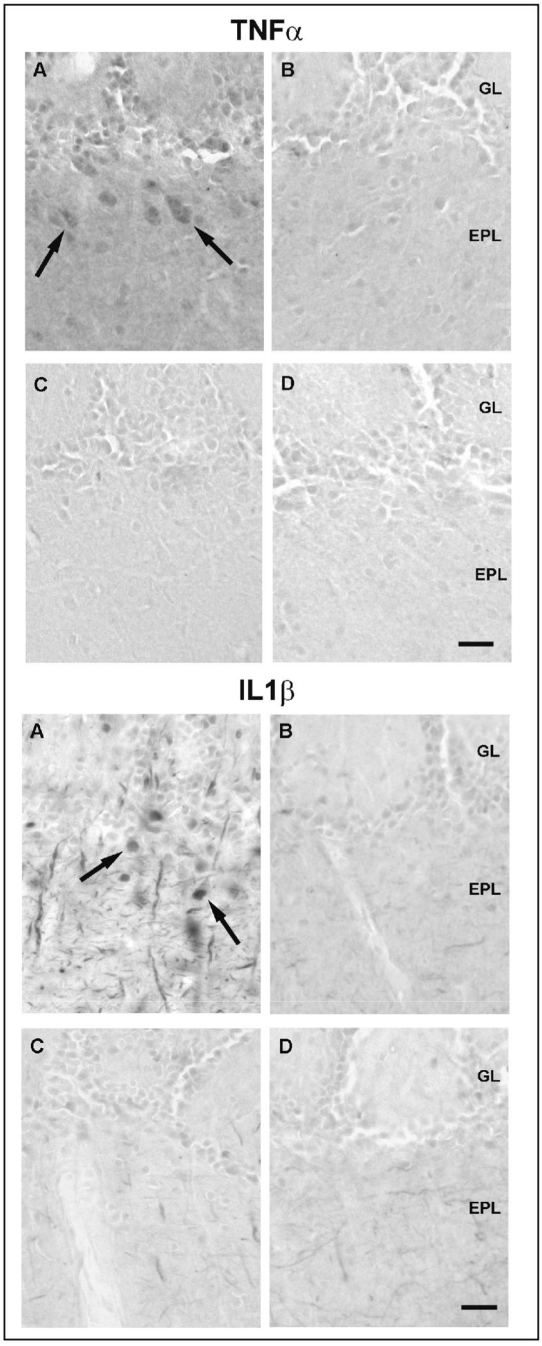

Fig. 1.

Demonstration of the specificity of cytokine antibodies used. Tumor necrosis factor alpha (TNFα)- (top) and interleukin-1 beta (IL1β)-IR cells (bottom) in the OB of non-infected wild-type (WT) mice (A and C) and knockout (KO) mice (B and D) for the respective cytokine. Immunoreactivity was observed in neuron-like cells in the glomerular layer and in the external plexiform layer in the WT mice [(A) in top and bottom] but not in the KO mice (B in top and bottom). Preabsorption of the specific antibodies with the recombinant proteins for 24 h blocked the immunostaining for both cytokines in both WT mice (C) (top and bottom). Scale bar = 0.025 mm.

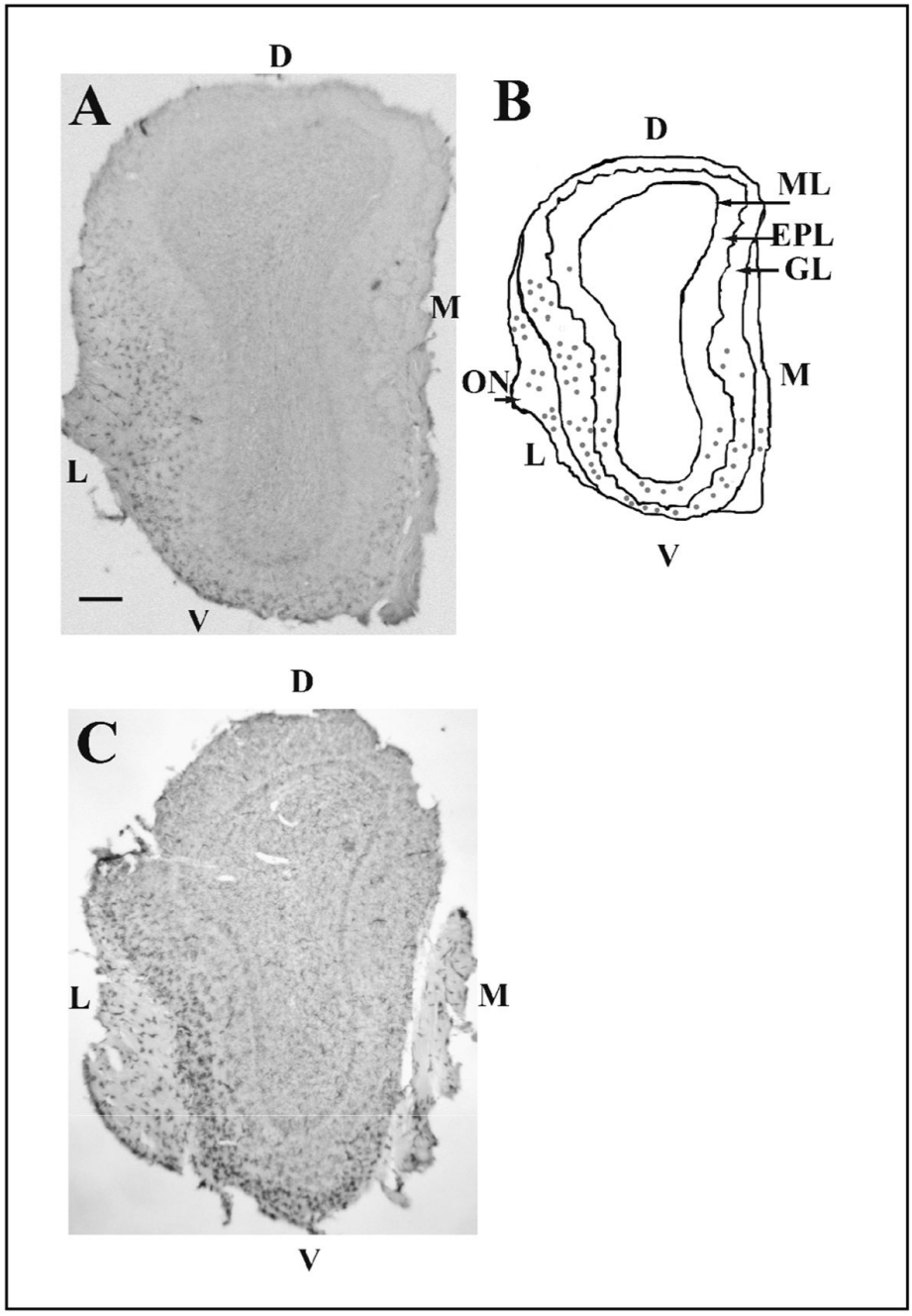

Fig. 2.

Distribution of viral protein and F4/80 immunoreactivity within cross-sections of the whole olfactory bulb (OB). Viral H1N1 immunoreactivity is mainly present in the olfactory nerve (ON) and glomerular layer (GL) with less detectable immunoreactivity in deeper layers such as the external plexiform layer (EPL) (A and B). The H1N1 immunoreactivity is largely concentrated in the ventro-(V) lateral (L) area of the OB (A and B). Fig. 2B is a schematic representation of the OB section in (A). Each dot represents two H1N1-IR cells (B). F4/80 immunoreactivity in the olfactory bulb showed a similar pattern of distribution to the one observed for the viral antigen (C). Scale bar= 0.2 mm. Mitral layer (ML), medial surface (M), and dorsal surface (D).

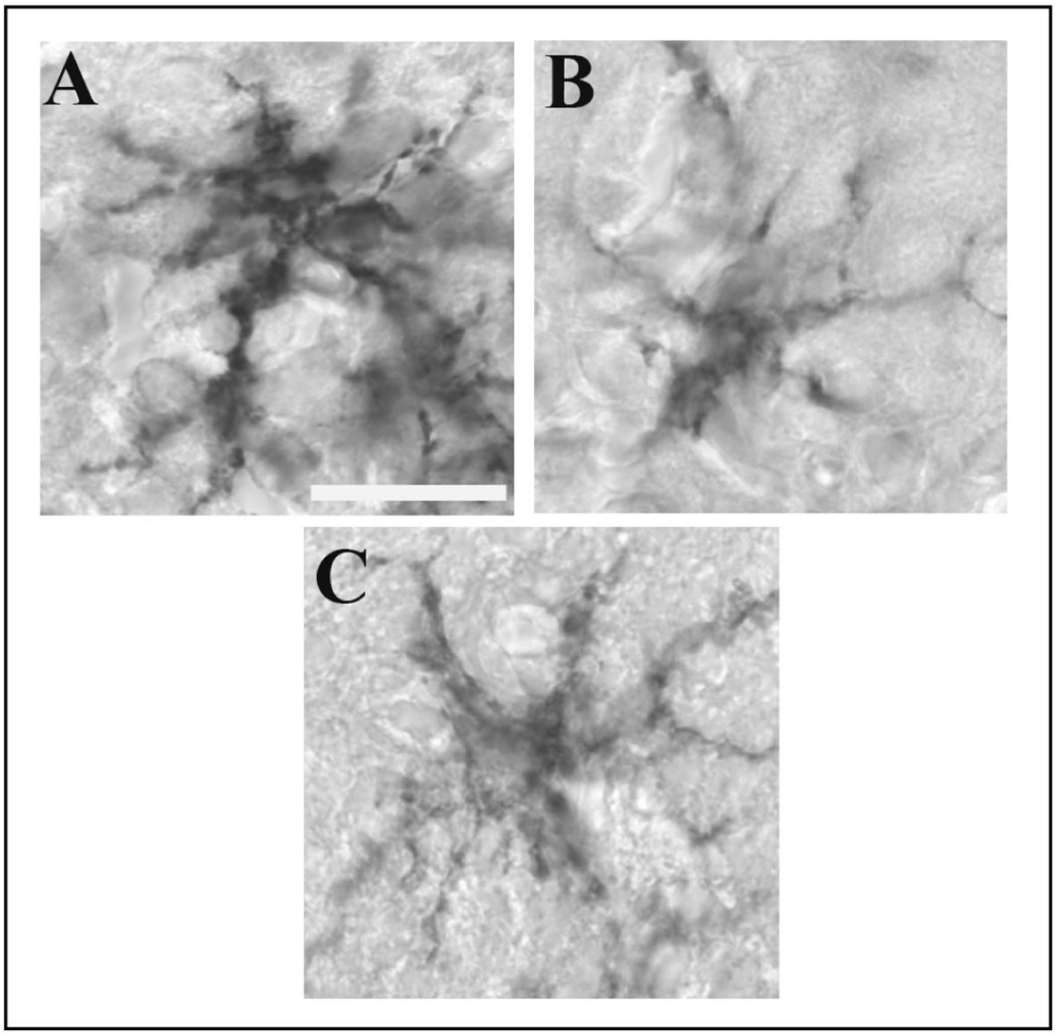

Fig. 3.

Morphological comparison of immunoreactivity in the glomerular layer of the OB sections of mice inoculated with live PR8 using F4/80 antibody (A), viral H1N1 antibody (B) and viral nucleoprotein (NP) antibody (C), respectively. Viral protein-IR cells (B and C) showed similar shape and size to the F4/80-IR cells (A), including several darkly stained processes. Scale bar = 0.01 mm.

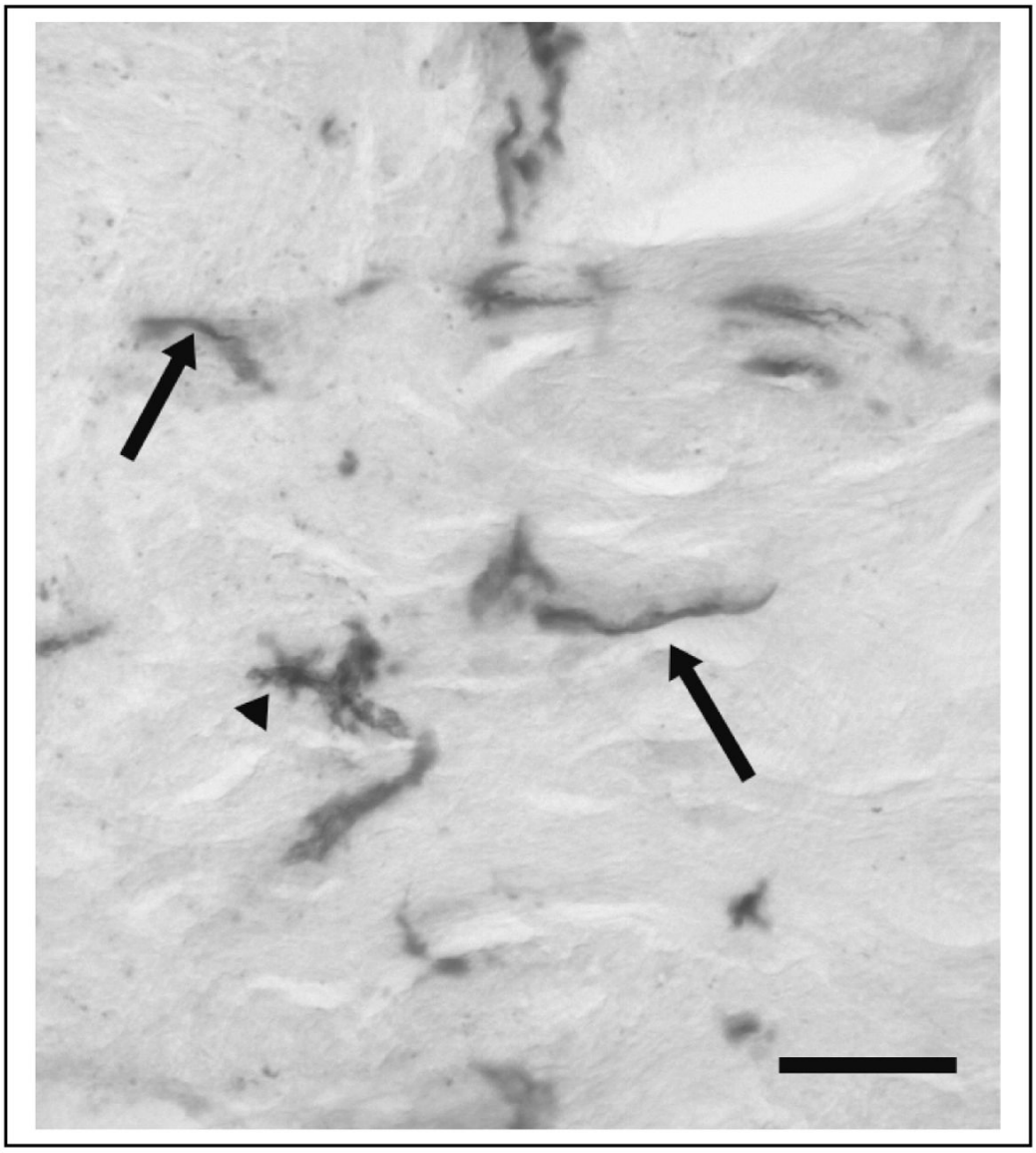

Fig. 4.
Photomicrograph of H1N1-immunoreactivity in the olfactory nerve of a mouse inoculated with live PR8. Arrows designate fusiform cells running along the nerve fibers. These H1N1-IR cells resemble olfactory ensheathing cells (Ubink et al., 1994). An arrow head illustrates H1N1-IR in a glia-like cell. Scale bar = 0.025 mm.

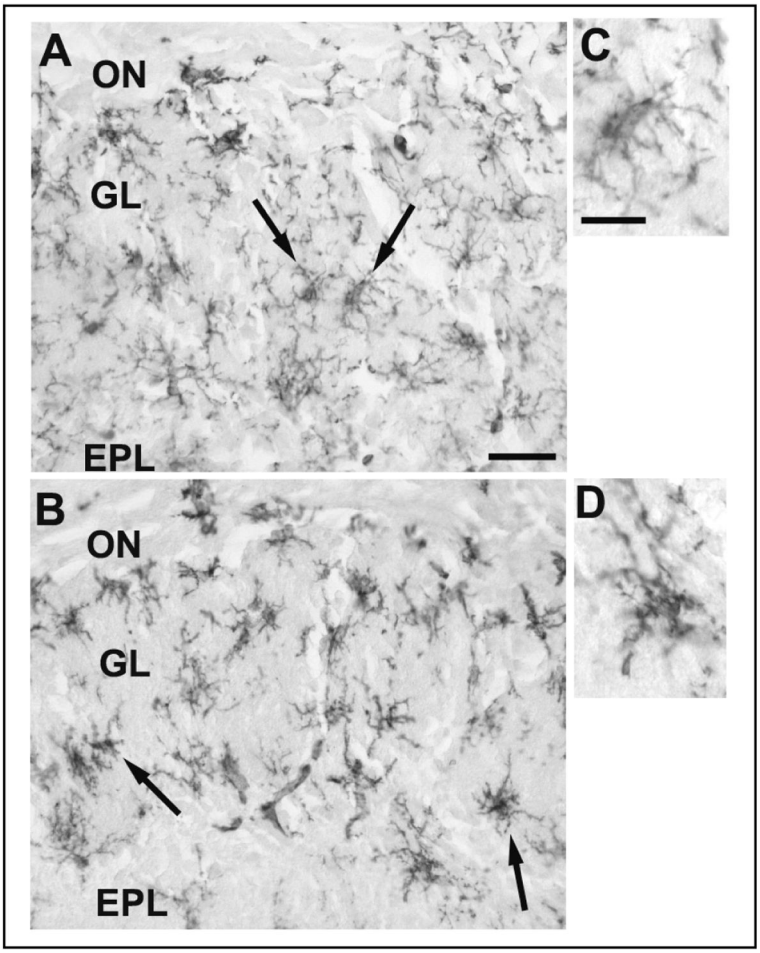

Fig. 5.

Photomicrographs of the olfactory nerve (ON), glomerular layer (GL) and external plexiform layer (EPL) of the OB from boiled and live virus-inoculated mice at 15 h post IN inoculation stained for F4/80 at two magnifications. At the lower magnification numerous intensely-stained ramified microglia-like cells (arrows) were seen in the GL and EPL of the OB of mice challenged with boiled (A) or live (B) PR8. Higher magnifications of the microglia-like cells are also shown for the boiled (C) and live (D) PR8-infected mice. Cells in the OB of mice inoculated with live virus (B and D) were more darkly stained and showed thicker processes than the cells in the OB from mice inoculated with boiled virus (A and C). Scale bar = 0.025 mm (A & B) or 0.01 mm (C & D).

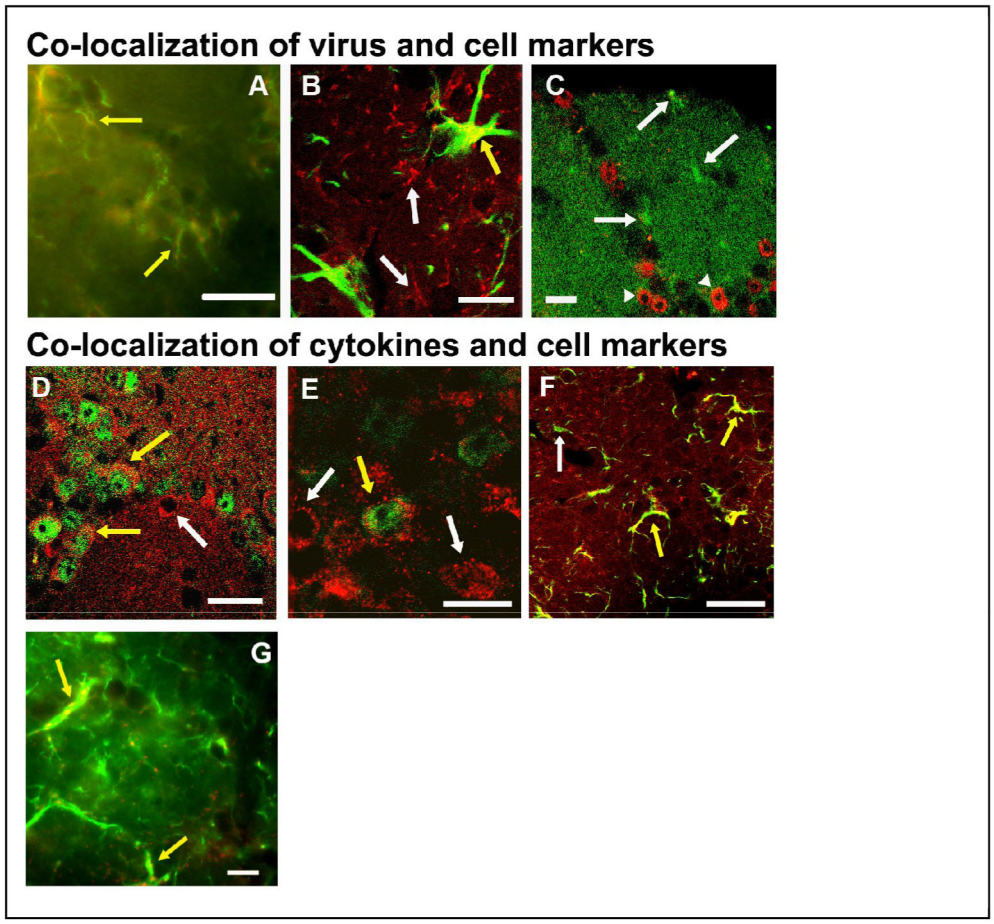

Fig. 6.

Immunofluorescence of H1N1-IR cells and cytokines with cellular markers is illustrated by light (A and G) or confocal (B, C, D, E, and F) photomicrographs of the OB of mice at 15 h after live PR8 inoculation. Yellow arrows indicate co-localization, while white arrows indicate single-labeled cells. Viral H1N1-immunoreactivity (red) co-localized with F4/80-immunoreactivity (green), suggesting that microglia-like cells in the GL take up virus (A). Viral H1N1-immunoreactivity (red) co-localized with some cells expressing the astrocyte marker GFAP (green) in the GL, suggesting that astrocytes in the GL also take up virus (B). Double-labeling with anti-viral H1N1 antibodies (green) and the neuronal marker NeuN (red) in adjacent sections of the infected OB did not show co-localization of the virus within neurons in the GL (C). Two cells showing double-labeling (yellow arrows) with TNFα (red) and NeuN (green) indicate the presence of TNFα in the cytoplasm of some juxtaglomerular neurons in the external plexiform layer. Some cells only showed TNFα-immunoreactivity (white arrow) (D). IL1β-immunoreactivity (red) co-localized with one cell also labeled with NeuN (green) in the external plexiform layer, demonstrating that IL1β was present in some neurons (yellow arrow) (E). Some cells in the glomerular layer labeled with IL1β (red) also expressed GFAP (green) indicating the presence of IL1β in astrocytes of the infected OB (F). Some cells in the glomerular layer labeled with IL1β (red) also expressed F4/80 (green) indicating the presence of IL1β in microglia of the infected OB (G) Scale bar = 0.01 mm (A, B, E, G) or 0.02 mm (C, D, F).

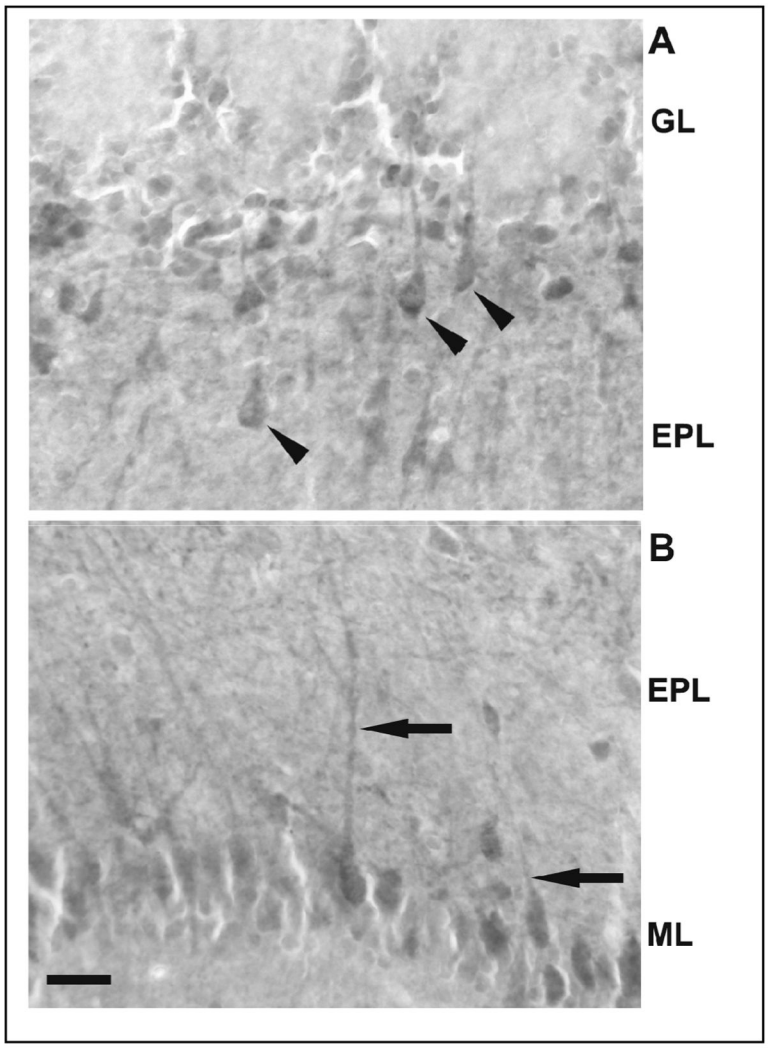

Fig. 7.

Tumor necrosis factor alpha (TNFα)-IR cells in the OB of mice inoculated with live PR8 15 h post inoculation. Immunoreactivity was observed in neuron-like cells (arrowheads) in the external plexiform layer (EPL) (A). TNFα-IR was also observed in the long neuronal projections (arrows) of mitral cells in the EPL (B). Scale bar = 0.025 mm. GL: glomerular layer; ML: Mitral cell layer.

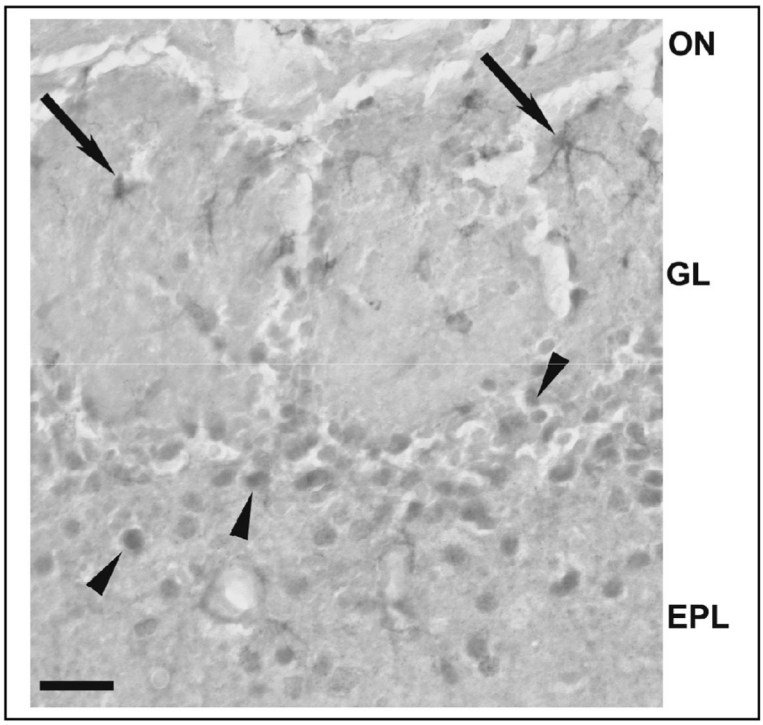

Fig. 8.

IL1β-immunoreactivity in the OB of mice inoculated with live PR8 virus 15 h post inoculation. The IL1β-immunoreactivity was observed in the GL and the EPL. The morphology of IL1β–IR cells suggests that both neuron-like cells in the EPL (arrow heads) and glia-like cells in the GL (arrows) are expressing this cytokine. Scale bar = 0.025 mm. ON: olfactory nerve.

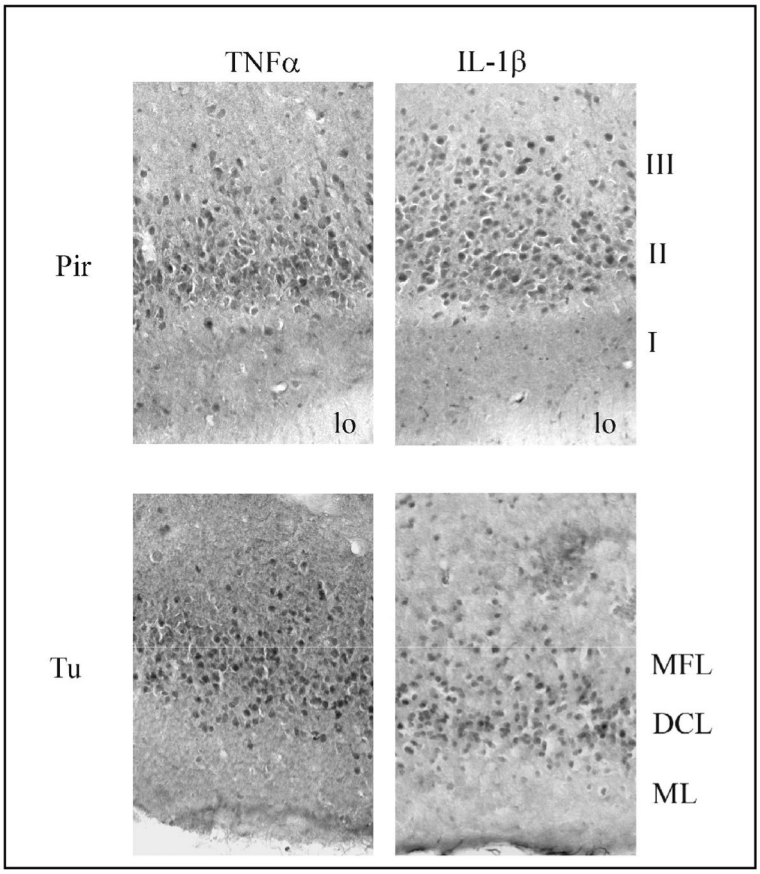

Fig. 9.

Distribution of the TNFα- and IL1β-immunoreactive (IR) cells in the piriform cortex (Pir) and olfactory tubercle (Tu) at 15 h after intranasal inoculation with live PR8 influenza virus. In the Pir, most of the IR-cells labeled with either cytokine antibody were observed in layer II. In the Tu, most of the IR-cells were observed in the dense cell layer (DCL). MFL (multiform layer), ML (molecular layer).

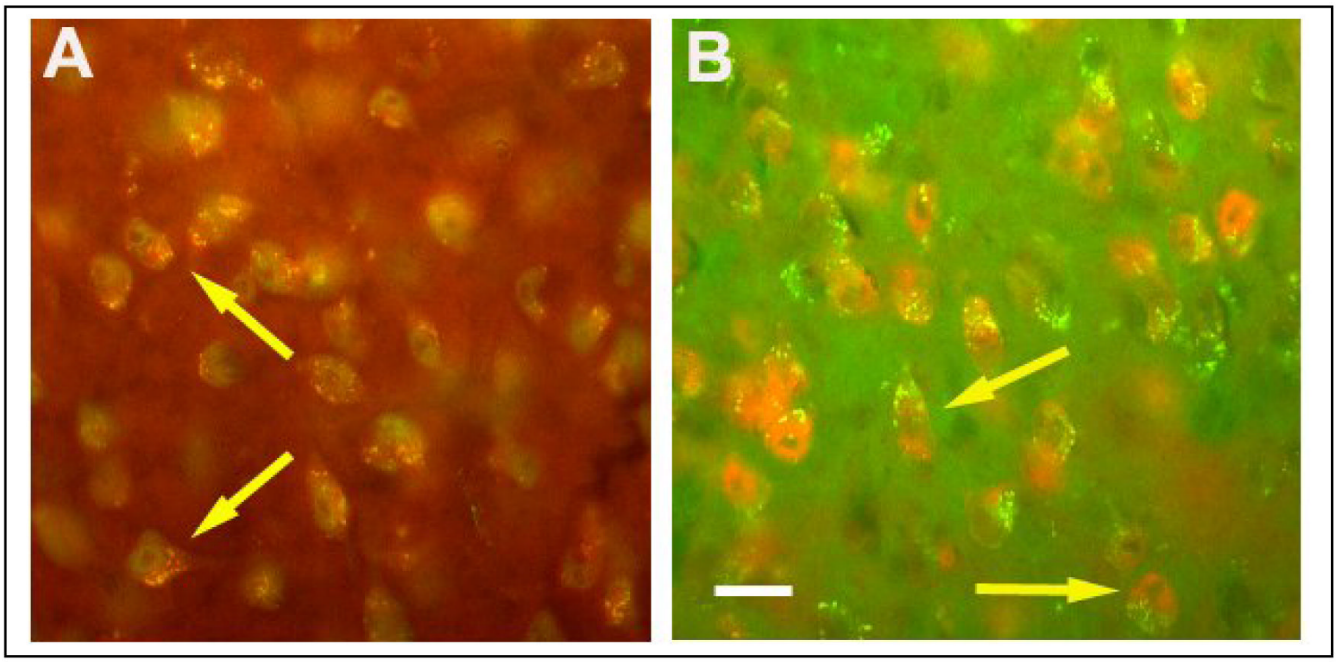

Fig. 10.

Immunofluorescence of TNFα–and IL1β-immunoreactive cells and the neuronal marker NeuN is illustrated by light microscopy in the central amygdala. TNFα (red) and NeuN (green) indicate the presence of TNFα in the cytoplasm of some neurons in the central amygdala from infected mice (A). IL1β-immunoreactivity (green) co-localized with cells also labeled with NeuN (red) in the central amygdala (B). Scale bar = 0.02 mm.

Table 1

Quantitative evaluation of the number of TNFα-IR cells in specific brain regions at 10 or 15 h following Boiled- or Live-PR8 challenge. Data are represented as Mean ± S.E.M. for 6 mice.

Brain Regions	Boiled 10 h	Live 10 h	p value	Boiled 15h	Live 15 h	p value	% of control
OB GL	73.6 ± 2.7	77.2 ± 4.9	0.23	33.7 ± 7.0	34.7 ± 2.4	0.23	
OB EPL	16.2 ± 3.0	13.8 ± 2.0	0.16	**15.7 ± 1.0**	**19.7 ± 1.1***	**0.005**	**25.5**
OB ML	11.0 ± 1.5	11.8 ± 1.2	0.64	**12.8 ± 1.3**	**16.0 ± 1.3***	**0.003**	**25.0**
Pir Ctx (Layer II)	12.0 ± 1.9	15.0 ± 2.2	0.2	30.5 ± 4.8	39.5 ± 6.9	0.08	
Olf Tub (DCL)	23.6 ± 4.5	25.5 ± 7.3	0.57	**31.1 ± 3.7**	**43.0 ± 2.5***	**0.02**	**38.3**
Sctx-layer II–IV	22.5 ± 3.0	24.3 ± 4.1	0.13	36.0 ± 3.1	39.3 ± 5.1	0.10	
Sctx-layer V	29.3 ± 3.4	30.1 ± 4.5	0.43	23.9 ± 2.1	27.0 ± 3.5	0.09	
BLA	4.6 ± 1.5	5.3 ± 2.0	0.28	10.7 ± 1.2	12.4 ± 1.6	0.6	
CeA	15.8 ± 2.7	19.3 ± 3.1	2.6	**30.4 ± 1.4**	**34.4 ± 2.1***	**0.05**	**13.2**
Hyp-Arc	19.1 ± 4.0	16.8 ± 1.9	0.6	23.4 ± 3.3	27.0 ± 5.9	0.23	

Table 2

Quantitative evaluation of the number of IL1β-IR cells in specific brain regions at 10 or 15 h following boiled or live PR8 challenge. Data are represented by Mean ± S.E.M. for 6 mice.

Brain Regions	Boiled 10 h	Live 10 h	p value	Boiled 15h	Live 15 h	p value	% of control
OB GL	17.1 ± 2.9	24.8 ± 5.3	0.08	38.0 ± 4.0	42.8 ± 2.5	0.072	
OB EPL	12.3 ± 1.3	10.5 ± 1.8	0.5	**15.8 ± 2.3**	**20.2 ± 1.8***	**0.006**	**27.8**
OB ML	19.0 ± 2.8	19.5 ± 1.9	0.86	12.3 ± 0.7	13.7 ± 1.2	0.09	
Pir Ctx (Layer II)	45.0 ± 7.6	43.6 ± 6.9	0.46	**48.7 ± 3.1**	**57.8 ± 3.3***	**0.02**	**18.7**
Olf Tub (DCL)	34.6 ± 10.9	26.0 ± 5.9	0.65	**28.1 ± 2.7**	**36.0 ± 2.7***	**0.04**	**28.1**
Sctx-layer II–IV	200.9 ± 24.7	196.3 ± 21.2	0.89	93.6 ± 10.0	94.2 ± 7.4	0.94	
Sctx-layer V	104.4 ± 9.4	113.9 ± 8.3	0.47	71.7 ± 8.9	72.2 ± 4.2	0.96	
BLA	19.8 ± 3.1	20.2 ± 2.3	0.39	21.1 ± 1.4	25.1 ± 2.1	0.06	
CeA	30.4 ± 1.4	23.5 ± 5.2	0.7	**33.2 ± 1.4**	**38.4 ± 1.6***	**0.03**	**15.7**
Hyp-Arc	32.0 ± 7.0	34.0 ± 3.6	0.43	**43.6 ± 2.7**	**56.0 ± 6.3***	**0.03**	**28.4**
Hyp-MPO	155.7 ± 12.1	190.6 ± 9.3	0.053	**119.2 ± 12.9**	**145.4 ± 13.5***	**0.041**	**22.0**